IEICE TRANS. FUNDAMENTALS, VOL.E106–A, NO.5 MAY 2023

PAPER Special Section on Analog Circuit Techniques and Related Topics

Pixel Variation Characteristics of a Global Shutter THz Imager and its Calibration Technique

Yuri KANAZAWA[†a)], **Prasoon AMBALATHANKANDY**[††], *Nonmembers*, *and* **Masayuki IKEBE**[††], *Member*

SUMMARY We have developed a Si–CMOS terahertz image sensor to address the paucity of low-cost terahertz detectors. Our imaging pixel directly connects to a VCO-based ADC and achieves pixel parallel ADC architecture for high-speed global shutter THz imaging. In this paper, we propose a digital calibration technique for offset and gain variation of each pixel using global shutter operation. The calibration technique gives reference signal to all pixels simultaneously and takes reference frames as a part of the high-speed image captures. Using this technique, we achieve offset/non-linear gain variation suppression of 85.7% compared to without correction.

key words: *terahertz, THz, CMOS imager, variation compensation*

1. Introduction

Electromagnetic waves in the terahertz band (100 GHz to 10 THz) have numerous characteristics that place them between the millimeter (mm) wave band and the infrared band. Terahertz waves have a higher spatial resolution than millimeter waves. Furthermore, terahertz radiation passes through a wide variety of materials, including plastics, fibers, and paper. The so-called fingerprint spectrum of terahertz frequencies can identify hazardous materials such as explosives, concealed weapons, and drugs. These capabilities have led to increased interest in terahertz imaging applications for medical [1], scientific imaging [2], and security screening [3].

In arrayed sensor applications, it is important to find out the difference of characteristics among all the sensors. When considering a THz image sensor, the variations of gain and offset on each pixel should be examined. However, there has been little discussion about variation correction methods for pixel arrays. Recently, many CMOS terahertz imagers have been proposed [4]–[8]. In order to suppress the manufacturing variations (MOSFETs threshold voltage variations), both offset and gain variations must be compensated. In this paper, we propose a calibration method for offset and gain variations in CMOS terahertz imagers, that are based on simulation and measurement results. Our contributions are following:

(i) Evaluation of the proposed imager from pixel level to array level.
(ii) Analysis of detail process variation effect in the proposed circuit.
(iii) Propose and evaluate a calibration method for the variations.

The rest of the paper is organized as follows; Section 2 describes the imager architecture; Section 3 presents mismatch variation. Our experimental measurement environment and results are discussed in Sect. 4. The proposed variation correction method is given Sect. 5 and the concluding remarks in Sect. 6.

2. Imager Architecture

Figure 1 shows the configuration of a 32×32 pixel-parallel THz imager. The imager integrates $32 \times 32 = 1024$ THz imaging pixels and an equal number of Voltage Controlled Oscillator (VCO) based ADCs. The pair of imaging pixels and VCO based ADC is hereafter referred to as the terahertz imaging unit (TIU). Each pixel and ADC corresponds to each other on a one-to-one basis. Therefore, all pixels can simultaneously perform imaging and high-speed A/D conversion. We have succeeded in high-speed imaging at 400 fps using this imager with a global shutter operation [9].

Figure 2 shows the circuit configuration of a terahertz imaging pixel. The terahertz imaging pixel consists of an on-chip antenna and a detection circuit. The detection circuit consists of two amplification circuits: a cascode amplifier (cascode amp) and a subthreshold operational amplifier

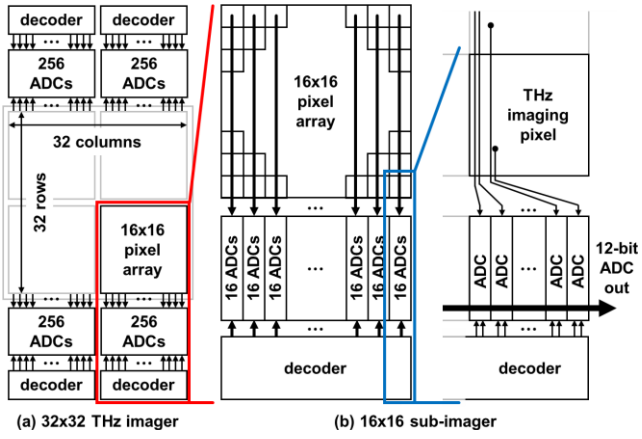

Fig. 1 Block diagram of THz imager.

Manuscript received May 25, 2022.
Manuscript revised September 20, 2022.
Manuscript publicized November 25, 2022.
[†]The author is with Graduate School of Information Science and Technology, Hokkaido University, Sapporo-shi, 060-0813 Japan.
[††]The authors are with RCIQE, Hokkaido University, Sapporo-shi, 060-0813 Japan.
a) E-mail: kanazawa.yuri.6z@ist.hokudai.ac.jp
DOI: 10.1587/transfun.2022GCP0004

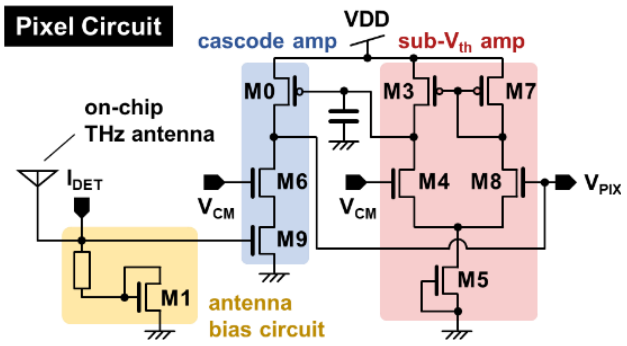

Fig. 2 Pixel circuit.

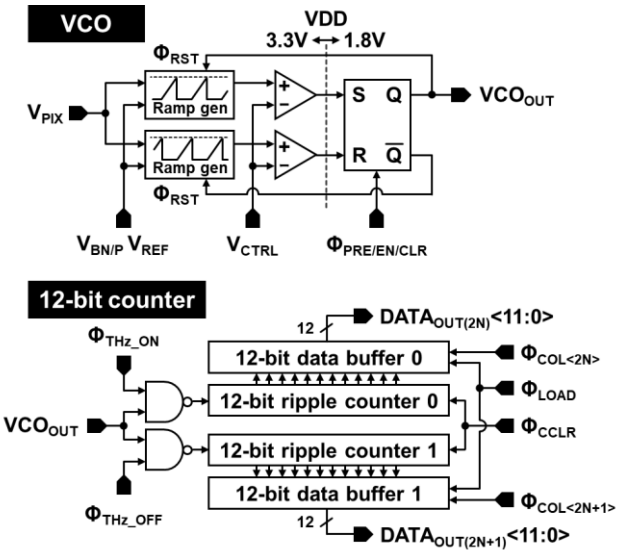

Fig. 3 VCO based ADC.

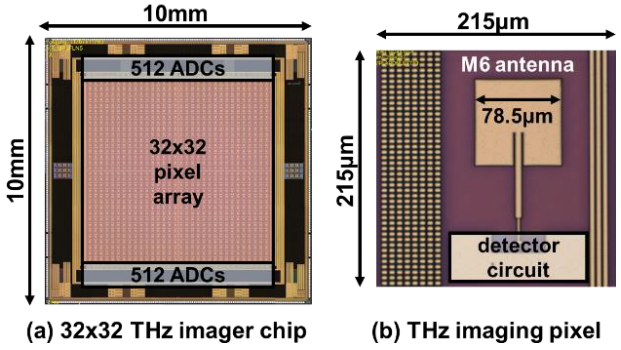

Fig. 4 Fabricated 32 × 32 THz imager.

(sub-Vth amp). The detection model using transistors has been previously analyzed by Kojima et al. and is described by the unified charge control model of FET channel carriers [10]. Self-mixing attenuates the AC component of the terahertz wave present at the source end of the channel, and the DC component is extracted at the drain end after mixing. Once transformed into the DC component, the channel does not contribute to detection and acts as a parasitic resistance. Thus, the OOK-modulated terahertz signal is envelope detected by the n-MOS in the input stage of the cascode amplifier. In the subthreshold operational amplifier, the n-MOS, which is the tail current source in the lower part of the op-amp, is driven by GND bias. Therefore, the cutoff frequency is about several tens of Hz. The waveform detected by the cascode amplifier has a DC component offset, but by applying negative feedback to the low-frequency component (~DC component) of this signal with the subthreshold operational amplifier and operating it as a DC servo, a waveform with a stable DC level can be obtained.

The structure of the VCO based ADC is shown in Fig. 3. This ADC can be divided into two subcircuits, a VCO and a counter. The VCO part in the first stage outputs a clock signal with an oscillation frequency corresponding to the input analog voltage. Two ramp generators in a single VCO, each determine the duty cycle of the clock high/low state. Certainly, small ramp generators can cause ramp noise, and in our proposed VCO, this ramp noise is the rising-edge/falling-edge jitter of the VCO output clock signal. Our VCO base ADC generates 1000~2000 cycles of clock signal continuously during a single A/D conversion (about 1 ms time). The resulting random jitter is integrated and averaged with other random jitter, so the total jitter of 1000~2000 clocks in one A/D conversion is smaller than the random jitter of a single clock. Since the random noise is reduced to $1/\sqrt{n}$ for an integration interval n, we used a small ramp wave source for our proposed VCO. The counter portion in the latter stage counts the number of rising edges of the input clock signal (equivalent to the frequency) over an arbitrary time width. The VCO performs analog-to-analog conversion from voltage to frequency, and the counter performs analog-to-digital conversion from frequency to count value. This ADC quantizes the input voltage. Additionally, this VCO based ADC has two sets of counters. This allows parallel A/D conversion in two arbitrary periods, and it is shown in Fig. 3, through A/D conversion each input value for the THz ON/OFF periods, it is possible to simultaneously obtain the signal level and background level required for correlated double sampling (CDS) operation.

2.1 32 × 32 Pixel Parallel CMOS THz Imager

Figure 4 shows a micrograph of our fabricated imager, and the microstrip patch antenna-type pixel [9]. Figure 5 shows measured characteristics of V_{PIX}, the output from THz imaging pixel. These noise and gain characteristics were measured with pixel circuit test element group (TEG) without any terahertz wave exposure. The measured noise and frequency characteristics are consistent with the post-layout simulation results. Since the pad simulation has parasitic capacitances, the gain in the simulations with it is lower than in the simulations without pad.

Figure 6 shows the experimental setup for the following measurement. An injection seeded terahertz wave parametric generator (is-TPG) is used as a frequency tunable terahertz wave source [11]. By changing the noncollinear phase matching condition in MgO:LiNbO3 crystal, the tera-

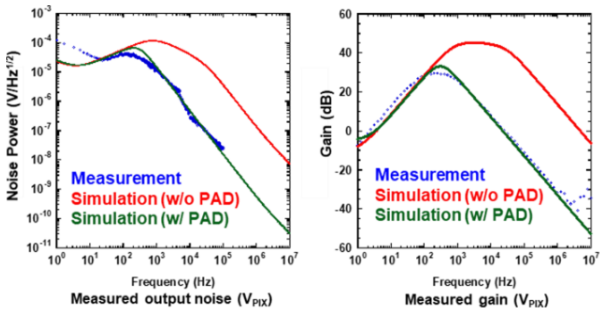

Fig. 5 Simulated and measured characteristics.

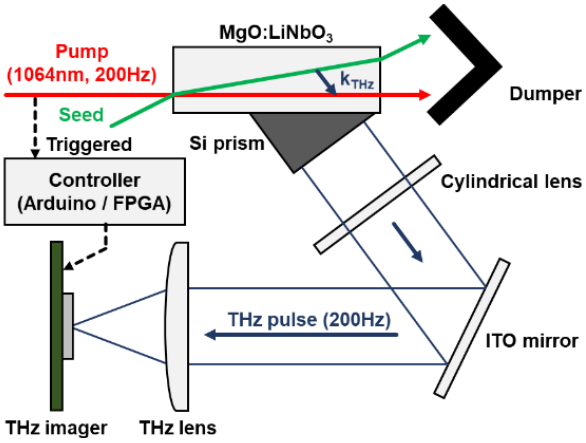

Fig. 6 Measurement environment.

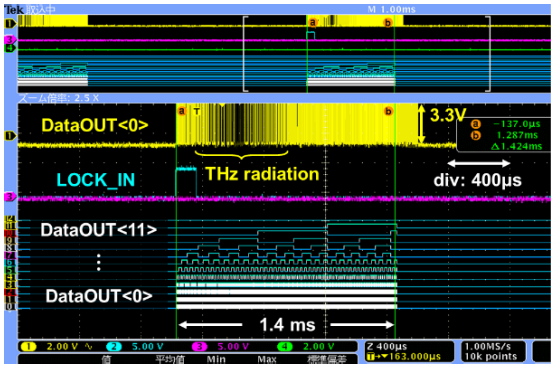

Fig. 7 Transient analysis of pixel and ADC.

hertz wave frequency was continuously tuned from 0.8 THz to 1.1 THz.

Figure 7 shows the transient characteristics of an ADC with the microstrip patch antenna-type pixel circuits. As shown in Fig. 8, the ADC control pulse (Φ_{THz_ON}) is generated in synchronization with the THz pulse. This operation is performed using an Arduino Uno board. The ADC is locked in with this pulse and the output is observed. When a terahertz wave is detected, we can observe the changes in frequency while monitoring the least significant bit voltage (LSB) of the ADC. Our ADC has monotonically increasing characteristics, because of its VCO based architecture.

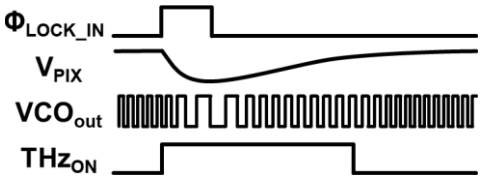

Fig. 8 Relation of the control signal and output.

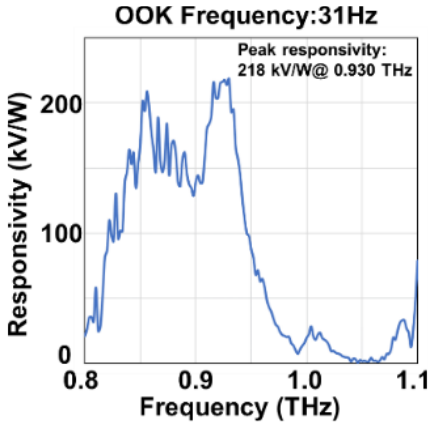

Fig. 9 Measured frequency responsivity characteristics.

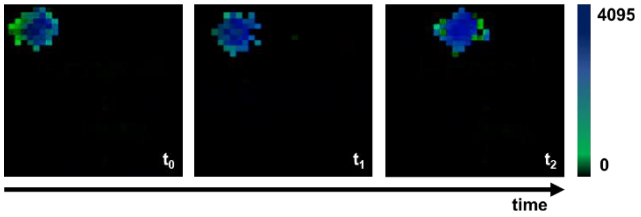

Fig. 10 Shifting THz beam spot (captured in 400 fps).

Therefore, good DNL characteristics is guaranteed and easy compensation of INL can be applied. The analog part which consists of the VCO, consumes 116 µW of power.

The terahertz beam has a Gaussian like form, average power is 18.8 µW@0.93 THz. We also confirm a responsivity of 218 kV/W@0.93 THz in the 78.5 µm × 78.5 µm antenna area and 34.6 kV/W@0.933 THz in the 215 µm × 215 µm detector area from the given Gaussian form beam profile (Fig. 9). The former responsivity is effective for interpolation-based image reconstruction because the antenna area is considered to sub sampling of whole image. Measured noise equivalent power (NEP) was 91 pW/Hz$^{0.5}$ @31 Hz, and 13.7 pW/Hz$^{0.5}$ @100 kHz was obtained as estimated NEP.

Figure 10 shows the working of our imager [9], by capturing an example image. Framerate is restricted by OOK modulation frequency of 200 Hz for the terahertz source. Actually, as a double of the OOK frequency, 400 frames (200 frames each for THz_ON and THz_OFF state) of images are being output. On the shifting beam spot, real-time capturing of the shift to the right direction is performed and its position is displayed in the image sequence. Table 1 com-

Table 1 Comparison table for recent THz imager.

	Sensors 2016[4]	IEEE THz Sci. 2016[5]	RFIT 2017[6]	ASSCC 2018[7]	ISSCC 2021[8]	our work[9]
CMOS Process	130nm	130nm	65nm	180nm	130nm	**180nm**
Array	31×31	8×8	7×7	32×24	32×32	**32×32**
Pixel pitch [μm x μm]	240×240	159×159	500×500	220×200	80×80	**215×215**
Power consumption [μW/pixel]	174	150	N/A	N/A	13.3	**4.5**
Antenna	Bow tie	Patch	Differential patch	Patch	Rectangular wire loop	**Patch**
Detection Device	MOSFET rectifier	MOSFET rectifier	MOSFET amplifier	MOSFET rectifier	MOSFET amplifier	**MOSFET amplifier**
Responsivity [V/W]	300k @270GHz	3.46k @820GHz	1.2k @303GHz	1.28k @860GHz	N/A	**218k @930GHz**
On-chip gain [dB]	58	13.5	N/A	N/A	139	**45**
ADC	External	External	External	N/A-bit Delta-Sigma	6-bit Flash	**12-bit VCO-Based**
Shutter	Focal plane	Focal plane	Focal plane	Focal plane	Focal plane	**Global**
NEP[pW/Hz$^{0.5}$]	18.7@156kHz	21.2@1MHz	20	N/A	262@40kHz	**91@31Hz**

pares our work with recently reported antenna type CMOS terahertz imager [4]–[8]. Almost all imagers use MOSFET rectifier in 65 nm or 130 nm CMOS process. They do not support A/D conversion or global shutter i.e. they are focal plane type. On the other hand, our imager applies pixel parallel ADC architecture using column ADCs and capture 2× images for digital correlated double sampling (digital CDS) while keeping high responsivity over 200 kV/W, low NEP and consumes low power in 180 nm CMOS process. Since the global shutter, is well known to reduce the image distortion while capturing movies. The pixel parallel architecture achieves higher framerate, which is practically useful for applications like multi frame super resolution.

3. Mismatch Variations

A terahertz detector functions with weak baseband signals, hence, requires some form of an in-pixel amplification [6], [8], [9], or it has to operate with modulated charge integration [4], [5]. Recently, efficient terahertz modulation based on total internal reflection for single-pixel imaging was reported in [12], however, there is some transparency loss in each coded aperture cell. Correlated double sampling (CDS) based offset calibration technique has been applied to the detector array as subtraction between reference/signal voltage, OOK frames, and use of differential configuration. However, there are little discussion on the gain variation. Here, we discuss and propose a gain calibration with our imager based on the experiments, simulation, and measurement results. In analog circuit elements, it is essential to consider mismatch variations. In our CMOS THz imager, mismatch variation between the analog circuit elements, a set of imaging pixel and VCO (which is a TIU), is considered to have a significant impact on the imager output. We performed Monte Carlo sampling simulations to estimate the mismatch variability of our imager and its contributing factors. Using the TIU circuit model, a steady-state bias value of 0.5 V was applied to the I_{DET} pin, which is the bias power supply for the THz antenna. Figures 11 and 12 show the distribution of the average output frequency when a steady-state bias value of 0.5 V is applied to the I_{DET} pin (THz_OFF) and when a 10 mV pulse signal is added to the

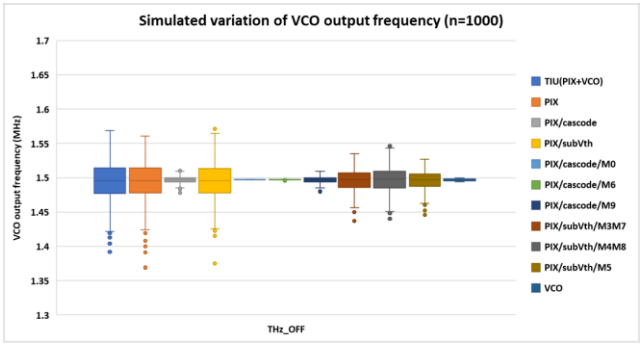

Fig. 11 Simulated VCO variation in THz OFF state.

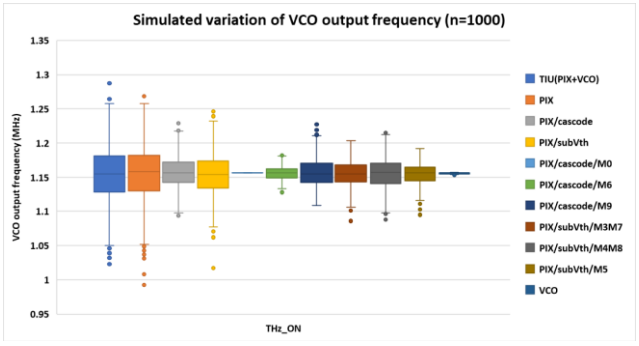

Fig. 12 Simulated VCO variation in THz ON state.

I_{DET} pin as a pseudo-input (THz_ON), respectively.

These figures are the simulated results of Monte Carlo sampling targeted to the entire TIU, the entire pixel circuit, one part of pixel circuit (cascode amplifier), another part of pixel circuit (subthreshold operational amplifier) and VCO. The variation at THz_OFF can be regarded as an offset variation. From these results, it can be seen that the variation in the pixel circuit section dominates the variation in the entire TIU, and the variation in the VCO has a small effect on the TIU. In the pixel circuit, results show that the variation of the cascode amplifier is small when THz_OFF and the variation increases when THz_ON. This indicates that the variation of the cascode amplifier causes the gain variation of the pixel circuit. In general, comparing the variation at THz_OFF and THz_ON, the variation at THz_ON tends to be larger than that at THz_OFF. This is thought to be due to both offset and gain variation in the output frequency of the TIU in THz_ON. The effect of the variation of each MOSFET in the pixel circuit is checked in more detail. For M9, M6, and M0, which constitute the cascode amplifier, the effect of variation is small for all MOSFETs at THz_OFF. This is because the DC servo by the subthreshold operational amplifier, as described in Sect. 2, suppresses the variation. Especially for M0, which is the negative feedback input from the subthreshold operational amplifier, the variation is almost completely suppressed. On the other hand, in the THz_ON state, the cascode amplifier determines the gain of the pixel circuit, so the effect of variation is significant. For the two differential pairs M3-M7, M4-M8 and

Table 2 Influence ratio of each circuit elements.

Circuit Element	THz_OFF	THz_ON
TIU(PIX+VCO)	1.000	1.000
PIX	1.006	1.006
PIX/cascode	0.163	0.564
PIX/subVth	0.926	0.782
PIX/cascode/M0	$< 10^{-12}$	$< 10^{-12}$
PIX/cascode/M6	0.016	0.227
PIX/cascode/M9	0.163	0.513
PIX/subVth/M3M7	0.551	0.465
PIX/subVth/M4M8	0.615	0.518
PIX/subVth/M5	0.451	0.385
VCO	0.030	0.029

the MOSFET M5 that make up the subthreshold operational amplifier, the variation does not change significantly between THz_OFF and THz_ON states. This means that offset variation is always occurring when the system is operating as a DC servo. Table 2 shows the ratio of the standard deviation during the variation of each element when the standard deviation during the overall variation is 1.

The ratio of "PIX" is larger than that of "TIU", due to the problem of simulation accuracy. Performing Monte Carlo sampling with 8000 samples, the ratio goes down to 0.972 (THz_OFF) and 0.987 (THz_ON).

4. Experiments

This section describes the measurement method used to measure the variation of imager output values for our 32 × 32 THz imager and the results.

4.1 Measurement Environment

Our experimental setup includes a THz imager evaluation board, an Arduino UNO board, a PC for handling Arduino and data acquisition, two Yokogawa GS820 (Power Supply Unit), and discrete circuits such as a level shifter IC and counter IC configured on the breadboard. This setup is shown in Fig. 13.

One cycle of measurement is shown in Fig. 14 and the measurement steps are the following (1→8).

1) Initialization of the entire THz imager (VCO initialization and start of free-run operation and counter initialization).
2) Start of pseudo input signal, start of VCO counter operation (start of A/D conversion).
3) End of pseudo input signal/end of VCO counter operation (end of A/D conversion).
4) Designation of read address (initial value 0) by address counter IC.
5) Readout of A/D conversion value (12-bit digital) at the specified address/data transfer to PC.
6) Input pulses to the address counter IC to advance the readout address by 1.
7) Repeat steps 5) and 6) to read out all 256 data and transfer to PC.
8) Initialize the VCO counter and return to 2).

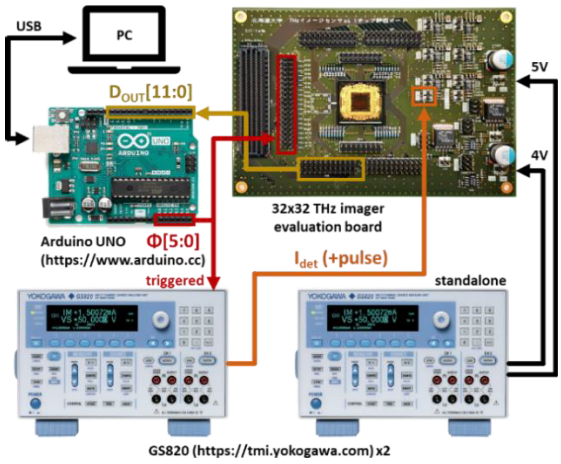

Fig. 13 Overview of measurement environment.

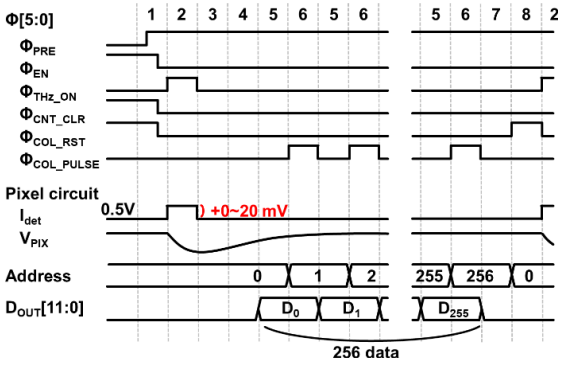

Fig. 14 Signal chart in single frame measurement.

The intensity of the pseudo-input signal (pulse wave) to the I_{DET} pin is set to 0 mV~20 mV in 2 mV increments. Our calibration method exploits the global shutter function of the pixel array. All pixels are simultaneously given a reference signal from an external DAC to perform the calibration image capture. Images out of 400 fps (= 10 in this paper) can also calibrate the non-linearity of the gain characteristics with respect to the input signal intensity.

4.2 Measurement Results

This section describes about measurement results of the fabricated terahertz imaging units (TIUs). 256 TIUs output data are measured in 16×16 sub-imager region shown in Fig. 15. For each 256 TIUs × 100 sets of data at each pseudo-input pulse intensity, the 100 sets of the data are averaged for each TIU. The distribution of this data is shown in Fig. 16. The measured output variations show a trend similar to the simulation results. When the intensity of input pulse is increased, the variations are also increase. In addition, the simulation results are verified only for a pulse intensity of +10 mV re-

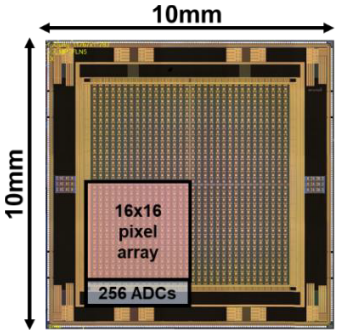

Fig. 15 Measured sub-imager region in chip micrograph.

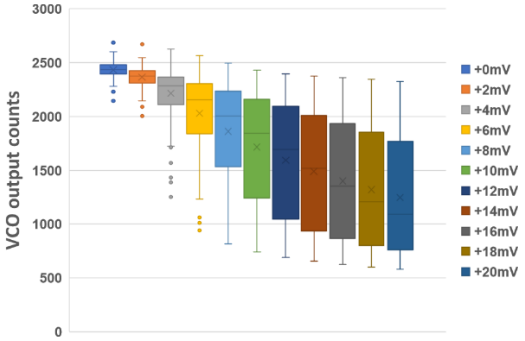

Fig. 16 Measured VCO variation with pseudo-input pulse.

stricted to the simulation time, but the actual measurements are made in the region from +0 mV up to +20 mV. This results in an increasing nonlinearity between input intensity and output data under conditions of high pulse intensity. However, comparing the past measurement data (Fig. 7) and this data (Fig. 16) shows that the actual THz OOK signal input is about several mV in terms of pseudo-input pulse intensity. Therefore, it is believed that the area of high nonlinearity where the counts are saturating is not used in the actual image sensor operation. Figure 16 shows a simplified set of input/output characteristics for this 256 TIUs x 11 data points as an independent 256 TIUs circuit. This figure also shows the occurrence of variation in both offset and gain.

Figure 17 shows an image representation of the 0 mV and 10 mV values in Fig. 16, effectively visualizing the offset variation in the 0 mV image and the gain variation in the 10 mV image. Figure 18 shows subtracted image of two images in Fig. 17. This image shows that gain variation cannot be suppressed by CDS alone.

In the next section, we describe a method for suppressing this input-output characteristic variation by post-measurement correction.

5. Variation Correction Method

In this section, we describe a post-processing method to suppress variations in the input/output characteristics of 256 TIUs. As shown in Fig. 19, offset and gain variations exist in the input-output characteristics of each TIU. Data(i) in Eq. (1) and Fig. 19 below is the measured output value of

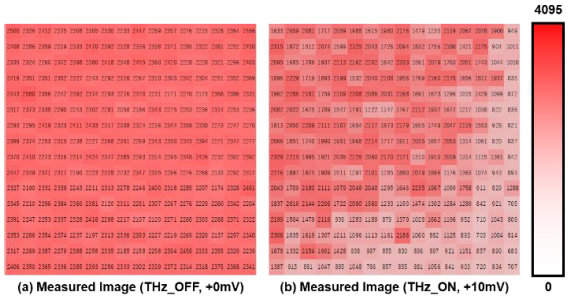

Fig. 17 Measured image (THz_OFF, THz_ON).

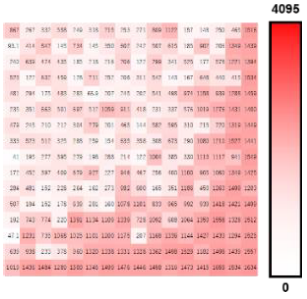

Fig. 18 CDS image ("THz_OFF" - "THz_ON").

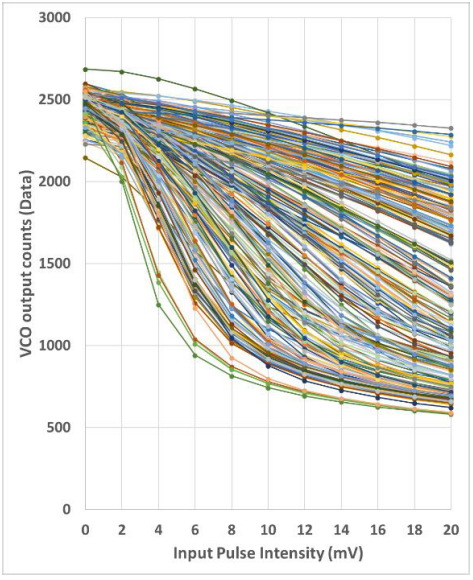

Fig. 19 Measured VCO characteristics.

each VCO at an i: an input pulse intensity described in mV unit. Values of ${}^{n}\mathrm{Data(i)}$ in Eqs. (1)~(4) and Figs. 20~22 represent the calculation results in n: the number of equations. For example, ${}^{2}\mathrm{Data(10)}$ is the calculated value by Eq. (2) at +10 mV input pulse intensity. "${}^{n}\mathrm{i}_{MAX}$" is the i that makes ${}^{n}\mathrm{Data(i)}$ the maximum value (${}^{n}\mathrm{Data}_{MAX}$).

First, to remove the offset in the steady state, the difference between the output value when the input pulse intensity is +0 mV and the output value when the input pulse intensity is +0 mV~+20 mV is taken (Eq. (1), Fig. 20).

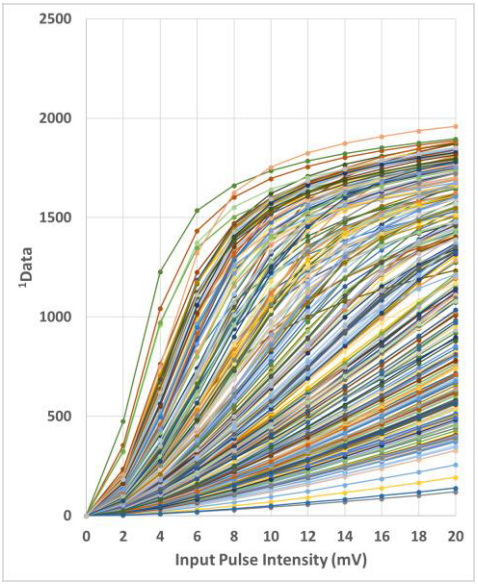

Fig. 20 Measured VCO characteristics with CDS.

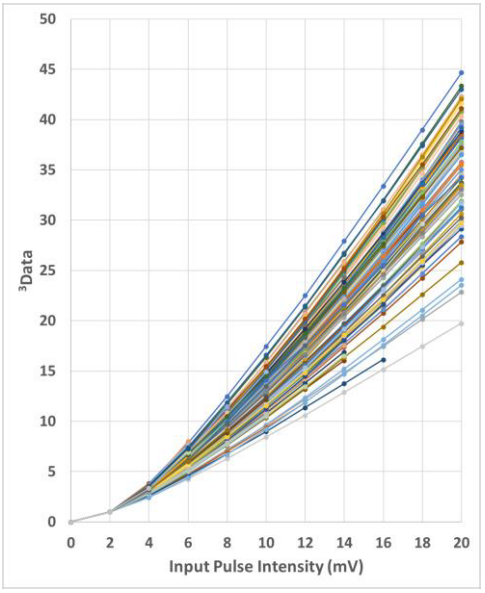

Fig. 21 VCO Characteristics Calculated with Eq. (3).

$$^{1}Data(i) = Data(0) - Data(i) \tag{1}$$

This technique of taking the difference between the background and signal input states is well known as correlated double sampling (CDS); CDS can remove the offset component from the input-output characteristics. We used the term "CDS" broadly as offset calibration. It is different from "True CDS" that considers time-correlated thermal noise and other factors.

Next, the data in the region where the counts tend to saturate (count > 750) are removed (Eq. (2)).

$$^{2}Data(i) = \begin{cases} ^{1}Data(i), ^{1}Data(i) \leq 750 \\ \text{“N/A”}, ^{1}Data(i) > 750 \end{cases} \tag{2}$$

As mentioned in the previous section, the region where the counts are becoming saturated is not used during the actual terahertz imaging operation, so there is no need to consider the input-output characteristics in this area. Next, a normalization is performed at the point where the pulse intensity is +2 mV (Eq. (3), Fig. 21).

$$^{3}Data(i) = \frac{^{2}Data(i)}{^{2}Data(2)} \tag{3}$$

This point reflects a large variation in response (=gain) to small input signals. Therefore, normalization at this point is expected to suppress gain variation over a wide range.

Finally, a curve fitting is performed (Eq. (4), Fig. 22).

$$^{4}Data(i) = \frac{^{3}Data(i)}{^{3}Data_{MAX}} \times \left(^{3}i_{MAX}\right)^{1.3\sim1.5} \tag{4}$$

By this process, the gain variation between TIUs can be suppressed. Comparing coefficients of variations in Figs. 20 and 22, there is an 85.7% decrease from 1.004@2 mV to 0.1438@2 mV. Each coefficient of variations is obtained by dividing its standard deviation by its mean at +2 mV input pulse intensity.

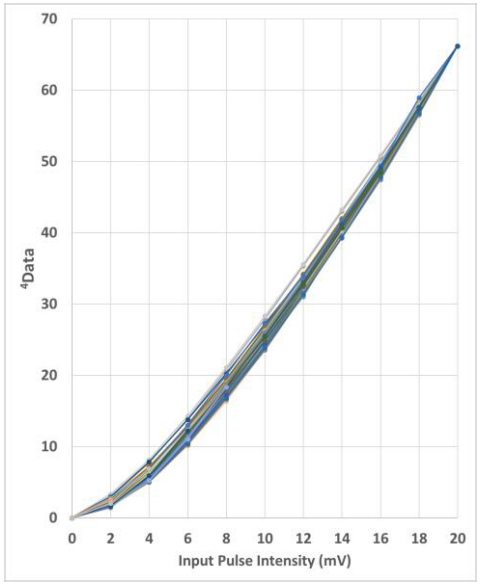

Fig. 22 VCO Characteristics Calculated with Eq. (4).

6. Conclusion

We designed, fabricated, and evaluated a pixel parallel ADC based CMOS global shutter THz imager in a 0.18-µm CMOS process. However, due to the gain variation in each pixel, pattern noises cannot be removed by CDS only. In this work, using Monte Carlo sampling simulations, we have identified the causes for pixel variation at MOSFET level. We also proposed a calibration method for offset and gain variations based on actual measurements of 16 × 16 pixels with ADCs. Using global shutter operation, we can simplify

reference signal distribution and get information for calibration. Using this technique, we achieved offset/non-linear gain variation suppression of 85.7% compared to without correction.

Acknowledgments

This work was partially supported by Grant-in-Aid for JSPS Research Fellow 20J2056102 and the VLSI Design and Education Center (VDEC), University of Tokyo in collaboration with Cadence Design System, Inc. and Keysight Technologies Japan, Ltd.

References

[1] P.U. Jepsen, D.G. Cooke, and M. Koch, "Terahertz spectroscopy and imaging–modern techniques and applications," Laser & Photonics Reviews, vol.5, no.1, pp.124–166, 2011.
[2] H.B. Liu, H. Zhong, N. Karpowicz, Y. Chen, and X.C. Zhang, "Terahertz spectroscopy and imaging for defense and security applications," Proc. IEEE, vol.95, no.8, pp.1514–1527, 2007.
[3] S.W. Smye, J.M. Chamberlain, A.J. Fitzgerald, and E. Berry, "The interaction between terahertz radiation and biological tissue," Phys. Med. Biol., vol.46, no.9, pp.R101–R112, 2001.
[4] R.A. Hadi, H. Sherry, J. Grzyb, Y. Zhao, W. Forster, H.M. Keller, A. Cathelin, A. Kaiser, and U.R. Pfeiffer, "A 1 k-pixel video camera for 0.7–1.1 terahertz imaging applications in 65-nm CMOS," IEEE J. Solid-State Circuits, vol.47, no.12, pp.2999–3012, 2012.
[5] D.Y. Kim, S. Park, R. Han, and K.O. Kenneth, "Design and demonstration of 820-GHz array using diode-connected NMOS transistors in 130-nm CMOS for active imaging," IEEE Trans. THz Sci. Technol., vol.6, no.2, pp.306–317, 2016.
[6] K. Song, J. Kim, D. Kim, M.G. Seo, and J.S. Rieh, "A CMOS 300-GHz 7 by 7 detector array for THz imaging," 2017 IEEE International Symposium on Radio-Frequency Integration Technology (RFIT), pp.31–33, 2017.
[7] T. Fang, R.J. Dou, L.Y. Liu, J. Liu, and N.J. Wu, "A 25 fps 32×24 digital CMOS terahertz image sensor," 2018 IEEE Asian Solid-State Circuits Conference (A-SSCC), pp.87–90, 2018
[8] R. Jain, P. Hillger, J. Grzyb, E. Ashna, V. Jagtap, R. Zatta, and U.R. Pfeiffer, "34.3 A 32×32 Pixel 0.46-to-0.75 THz light-field camera SoC in 0.13 µm CMOS," 2021 IEEE International Solid-State Circuits Conference (ISSCC), pp.484–486, 2021.
[9] S. Yokoyama, M. Ikebe, Y. Kanazawa, T. Ikegami, P. Ambalathankandy, S. Hiramatsu, E. Sano, Y. Takida, and H. Minamide, "5.8 A 32×32-pixel 0.9 THz imager with pixel-parallel 12b VCO-based ADC in 0.18 µm CMOS," 2019 IEEE International Solid-State Circuits Conference (ISSCC), pp.108–110, 2019.
[10] H. Kojima, D. Kido, H. Kanaya, H. Ishii, T. Maeda, M. Ogura, and T. Asano, "Analysis of square-law detector for high-sensitive detection of terahertz waves," J. Appl. Phys., vol.125, no.17, 174506, 2019.
[11] S. Hayashi, K. Nawata, T. Taira, J. Shikata, K. Kawase, and H. Minamide, "Ultrabright continuously tunable terahertz-wave generation at room temperature," Sci. Rep., vol.4, no.1, pp.1–5, 2014.
[12] R.I. Stantchev, X. Yu, T. Blu, and E. Pickewll-MacPherson, "Real-time terahertz imaging with a single-pixel detector," Nat. Commun., vol.11, no.1, pp.1–8, 2020.

Yuri Kanazawa received the B.S. degrees in Engineering from Hokkaido University in 2018 and the M.S. degrees in Information Science and Technology from Hokkaido University in 2020, respectively. He now with Graduate School of Information Science and Technology, Hokkaido University to study terahertz imaging devices and systems as a Ph.D. course student.

Prasoon Ambalathankandy received the M.S. degrees in Electrical Engineerin from University of Calgary in 2016 and the Ph.D. degrees in Electronics for Informatics from Hokkaido University in 2020, respectively. He now with Research Center for Integrated Quantum Electronics, Hokkaido University as a postdoctoral fellow to study image processing.

Masayuki Ikebe received the Ph.D. degrees in Engineering from Hokkaido University in 2000. He now with Research Center for Integrated Quantum Electronics, Hokkaido University as a professor to study Functional sensing devices and systems.